

Substitution case study

Replacing niobium by vanadium in nano-steels

Arechabaleta Guenechea, Zalao; Offerman, Erik

DOI

[10.1142/9789813271050_0010](https://doi.org/10.1142/9789813271050_0010)

Publication date

2019

Document Version

Final published version

Published in

Critical Materials

Citation (APA)

Arechabaleta Guenechea, Z., & Offerman, E. (2019). Substitution case study: Replacing niobium by vanadium in nano-steels. In E. Offerman (Ed.), *Critical Materials: Underlying Causes and Sustainable Mitigation Strategies* (pp. 193-221). (World Scientific Series in Current Energy Issues; Vol. 5). World Scientific. https://doi.org/10.1142/9789813271050_0010

Important note

To cite this publication, please use the final published version (if applicable).
Please check the document version above.

Copyright

Other than for strictly personal use, it is not permitted to download, forward or distribute the text or part of it, without the consent of the author(s) and/or copyright holder(s), unless the work is under an open content license such as Creative Commons.

Takedown policy

Please contact us and provide details if you believe this document breaches copyrights.
We will remove access to the work immediately and investigate your claim.

World Scientific Series in Current Energy Issues **Volume 5**

Critical Materials

Underlying Causes and Sustainable Mitigation Strategies

Published by

World Scientific Publishing Co. Pte. Ltd.

5 Toh Tuck Link, Singapore 596224

USA office: 27 Warren Street, Suite 401-402, Hackensack, NJ 07601

UK office: 57 Shelton Street, Covent Garden, London WC2H 9HE

Library of Congress Cataloging-in-Publication Data

Names: Offerman, S. Erik, editor.

Title: Critical materials : underlying causes and sustainable mitigation strategies / S. Erik Offerman, Delft University of Technology, The Netherlands.

Description: New Jersey : World Scientific, [2018] | Series: World Scientific series in current energy issues ; volume 5 | Includes bibliographical references and index.

Identifiers: LCCN 2018028408 | ISBN 9789813271043 (hardcover)

Subjects: LCSH: Raw materials--Research. | Strategic materials--Research. | Mineral industries--Environmental aspects. | Sustainable engineering.

Classification: LCC TA404.2 .O43 2018 | DDC 333.8--dc23

LC record available at <https://lcn.loc.gov/2018028408>

British Library Cataloguing-in-Publication Data

A catalogue record for this book is available from the British Library.

Copyright © 2019 by Author

This is an Open Access ebook published by World Scientific Publishing Company and distributed under the terms of the Creative Commons Attribution (CC-BY) Licence.

For any available supplementary material, please visit

<https://www.worldscientific.com/worldscibooks/10.1142/11007#t=suppl>

Typeset by Stallion Press

Email: enquiries@stallionpress.com

Printed in Singapore

Chapter 10

Substitution Case Study: Replacing Niobium by Vanadium in Nano-Steels

Zalóa Arechabaleta Guenechea and S. Erik Offerman
*Department of Materials Science & Engineering,
Delft University of Technology, Mekelweg 2,
2628 CD Delft, The Netherlands*

The substitution of critical alloying elements in metals is a strategy to reduce the criticality of materials. Nano-steels are a novel grade of advanced high-strength steels that are suited for application in the chassis and suspension of cars and as fire-resistant steel in high-rise buildings. The high strength and ductility per unit mass make the nano-steels resource-efficient and reduce vehicle weight while maintaining crash worthiness. The excellent mechanical properties of certain nano-steels rely on the addition of small amounts (up to 0.1 wt.%) of Niobium as alloying element to the steel. Niobium is considered to be a critical raw material by the European Union due to its high economic importance as an alloying element in advanced, high-strength steel grades and due to the high supply risk related to the high degree of monopolistic production within the supply chain. This chapter describes the fundamental materials science that is needed for the substitution of the critical alloying element Niobium by Vanadium as an alloying element in nano-steels.

10.1 Introduction

The world population is expected to grow by about 30% by 2050 to approximately 9 billion people¹ and with people in emerging countries aspiring to the same lifestyle as in developed countries, the supply of resources is no longer guaranteed in the long term. Europe promulgates “resource-efficiency” as a key factor to address this challenge in the coming years and has established new enduring strategies in areas such as energy, climate change, research and innovation, industry, and transport, among others.¹ Promoting and assuring a secured, sustainable and sufficient supply of raw materials is of primary importance for the European Union (EU), as these

© 2019 The Authors. This is an Open Access chapter published by World Scientific Publishing Company. It is distributed under the terms of the Creative Commons Attribution (CC-BY) License which permits use, distribution and reproduction in any medium, provided that the original work is properly cited.

materials play an essential role in the EU's economy, growth, and competitiveness: key economic sectors including automotive, aerospace, and construction, strongly connected to the steel industry, are directly linked to their supply.

After China, the EU is the second largest producer of steel in the world, producing 11% of the global output.² "Resource efficiency" in the steel industry implies, among other challenges, the reduction of energy consumption and CO₂ emissions, both directly, via modification and/or improvement in the steelmaking process, and indirectly, by providing the best suitable steel solution for a specific use. An example of the latter is the use of Advanced High Strength Steels (AHSS) for lightweight automotive applications. These types of steels, exhibiting superior strength and formability, are extremely useful for improving fuel economy and reducing greenhouse gas emissions without compromising crash worthiness. In general, it can be claimed that using steel with higher strength helps to save steel: even partial global switching to higher strength steel could save 105 million metric tons of steel a year and 20% of the costs of steel.³

In view of the above, the steel industry worldwide is developing AHSS to satisfy the most exigent requirements in diverse applications. Nonetheless, conventional AHSS are not always adequate for high-tech applications despite their good strength-ductility balance. In the automotive industry, for instance, new chassis and suspension designs require, in addition, stretch-flangeability and bendability.

This enhanced combination of mechanical properties cannot be obtained with conventional AHSS grades that have a multiphase microstructure. The reason for this is that voids and cracks are formed in the multiphase steels during blanking and stretch-flanging, due to stress localization at the interface between the hard phases (*e.g.* martensite, bainite and retained austenite) and the soft ductile ferrite. To overcome this hurdle, the steel industry has recently developed the so-called nano-steels, *i.e.* a new generation of AHSS. Interestingly, this new type of steel can successfully be used for advanced applications, such as specific automobile parts, particularly those parts that are important for safety, and high-rise buildings for fire resistance. In contrast to conventional AHSS, their microstructure consists of a single soft ferritic matrix, providing ductility, strengthened by nanometer-sized precipitates. The very small size of the precipitates (the hard phase in this type of steels) dispersed in the ferritic matrix is critical to achieve the excellent mechanical behavior. Figure 10.1 schematically shows the microstructures of (a) a nano-steel with interphase

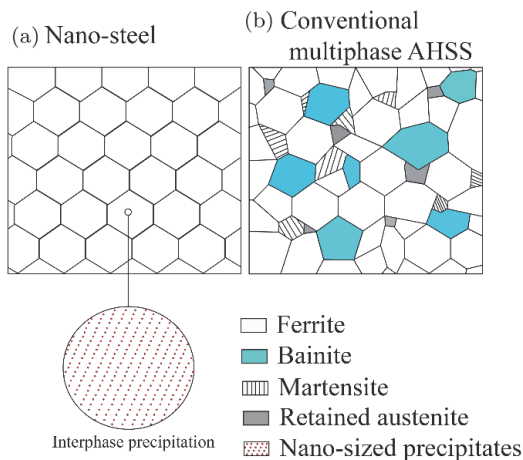


Fig. 10.1. Microstructures of (a) nano-steel and (b) conventional AHSS.

precipitation and (b) a conventional multiphase AHSS containing a small fraction of bainite, martensite and retained austenite embedded in ferrite. Besides their outstanding mechanical behavior, an additional advantage of nano-steels is that they can be produced by direct cooling from austenite at high temperatures, avoiding additional and expensive heat treatments and saving energy. This is not the case for the multiphase AHSS, which are usually produced by other thermal treatments.

Nano-steels use considerable microalloying additions, including Niobium (Nb, ≤ 0.1 wt.%), Titanium (Ti, ≤ 0.35 wt.%), Vanadium (V, ≤ 0.45 wt.%) and Molybdenum (Mo, ≤ 0.7 wt.%), to form the essential precipitating species,⁴⁻¹⁰ that is, the corresponding carbides and/or carbonitrides (MC and/or M(C,N), where M=Nb, Ti, V and Mo). Albeit these contents do not seem very high at first, they imply significant amounts of microalloying additions considering the large volume of steel produced worldwide. The microalloying elements are usually expensive, meaning that the commercial and industrial implementation of nano-steels is subjected to the efficient use of these elements, and hence, to the better understanding of the precipitation reactions involved. The first nano-steels that have been developed for automotive applications are based on additions of Ti and Mo¹¹: the Ti precipitates in the form of (Ti,Mo)C particles and the Mo suppresses TiC-precipitate coarsening (Ostwald ripening), keeping the precipitates small during processing. Other studies have also demonstrated a similar effect of Mo on NbC-precipitates.^{12,13} Yet, quantitative data

about the Mo effect on the TiC- and NbC-precipitation kinetics remains insufficient. Moreover, the EU has recently identified Nb as a critical raw material because its supply risk is high.¹⁴ The challenge is thus to design nano-steels that are: (1) more “resource-efficient”, by reducing and optimizing the microalloying additions, (2) containing less or no critical raw materials, and (3) at the same time maintaining or improving their excellent mechanical properties.

Vanadium is a promising candidate to (partially) replace Nb and Ti in nano-steels. The advantages of this element will be enumerated through this chapter. In contrast to Nb and Ti, the larger solubility of V can be exploited for different purposes, but mainly to optimize ferrite strengthening via precipitation of V(C,N). Literature on V-precipitation has provided compelling evidence that by using high Nitrogen (N) levels precipitate coarsening can be suppressed due to the reduced solubility of V(C,N) compared with VC in ferrite, which further enhances the precipitate hardening contribution. By contrast, little or nothing has been reported so far about the interaction between V and Mo, and the question to answer in the near future is if V, N, and Mo is the perfect combination for nano-steels.

From the abovementioned it can be concluded that dispersion of V(C,N) nanometer-sized precipitates is the most promising strategy to maximize precipitation strengthening and at the same time minimize the addition of alloying elements. This, however, is not straightforward and requires a deep understanding of how precipitation and the austenite to ferrite ($\gamma \rightarrow \alpha$) phase transformation interact, since both phenomena occur within the same range of temperatures during thermomechanical processing of nano-steels. In some cases, the precipitates will form at the austenite/ferrite (γ/α) interface as phase transformation proceeds. This is known as interphase precipitation (IP) and usually recognized by rows of aligned precipitates. In other cases, the precipitates will nucleate randomly from supersaturated ferrite. Different microalloying elements not only will generate different precipitation reactions with distinct kinetics, but also will influence the phase transformation (kinetics) in a different manner, which will affect the precipitation indirectly as well. Until now, it has proven to be impossible to disentangle the kinetics of both reactions, which indicates the great importance of in-situ and simultaneous use of advance characterization techniques, such as High-Resolution Transmission Electron Microscopy (HR-TEM), 3D X-ray Diffraction (3DXRD), Small Angle X-ray Scattering (SAXS), Small Angle Neutron Scattering (SANS), Neutron Diffraction (ND) and Electron Back Scattered

Diffraction (EBSD), among others, to enable precipitation optimization in nano-steels.

10.2 Nano-steels in High-tech Applications

In the following two sections, the main applications so far of nano-steels are elaborated, viz. structural fire-resistant steels and chassis and suspension systems. Note, however, that these steels are also suitable to substitute conventional High Strength Low-Alloy (HSLA) steels in other applications, for example. in oil and gas pipelines, farm machinery, industrial equipment, bridges and so on, provided that application requirements, if necessary, are satisfied, e.g. corrosion resistance, weldability, abrasion resistance, low-temperature impact toughness for line pipe and lifting and excavating applications, and fatigue properties for chassis.

10.2.1 Fire-resistant steels

Fire-resistant steels are structural steels, *i.e.* steels used in building constructions, which must guarantee sufficient strength at elevated temperatures to ensure that all internal and external loads applied to the structure can be carried. The exact criterion defining sufficient strength changes between different countries depending on their specific fire safety regulations. In Japan, for instance, the standards require that the yield strength (0.2% proof stress) of the steel at 600°C is at least two thirds of that specified at room temperature.¹⁵ Less stringent regulations in Australia, United States and Europe, demand in such conditions at least one half of the room temperature yield strength.^{16–18} For this type of steels, the yield strength can theoretically be calculated using the following equation¹⁹:

$$\sigma_y = \sigma_0 + \sigma_{ss} + \sigma_{gb} + \sqrt{\sigma_{dis}^2 + \sigma_{ppt}^2} \quad (1)$$

where σ_0 is a friction stress and σ_{ss} , σ_{gb} , σ_{dis} and σ_{ppt} are respectively contributions from solid solution, grain boundary, dislocation and precipitation strengthening. In other words, the strength of a steel can be tailored by modifying and optimizing its microstructure, *e.g.* varying the elements in solid solution and solute contents, the microstructure grain size and density of grain boundaries, the dislocation density and the volume fraction and size of precipitates. The main reasons why a steel loses its strength at high temperature are indeed related to how the different

terms in equation (1) evolve with temperature. These can be summarized as follows:

- *Enhanced mobility of dislocations.* At high temperatures, dislocations are activated by thermal energy and can easily move: dislocation glide, climb and cross slip are facilitated. When two dislocations of opposite sign encounter each other on the same slip plane, dislocation annihilation occurs. This mechanism can significantly reduce the dislocation density at elevated temperatures, and hence, lower the dislocation strengthening contribution. Note that $\sigma_{dis} \propto \rho^{1/2}$, where ρ is the dislocation density.
- *Precipitate coarsening.* The high interfacial energy of small precipitates provides the driving force for precipitate coarsening, which occurs by diffusion of solute atoms. Basically, the smallest precipitates shrink and dissolve in the steel matrix and the solute redistributes to the largest stable precipitates (Ostwald ripening), which increases the average particle size. Particle sizes larger than a critical value r^* , will cause the strengthening contribution $\sigma_{ppt} \propto r^{-1}$, where r is the average particle radius, to decrease (see Fig. 10.12). Moreover, as the temperature increases, diffusion is enhanced and the rate of precipitate coarsening is accelerated.
- *Microstructure coarsening.* The mobility of grain boundaries also increases with temperature. Grain coarsening will occur in case the solute content is not high enough and/or the precipitates are not sufficiently small to pin the grain boundaries. According to the well-known Hall-Petch relation, $\sigma_{gb} \propto d^{-1/2}$, in which d is the average grain diameter, a coarser microstructure will provide a smaller grain boundary strengthening contribution. The reason is that grain boundaries are less effective in hindering the migration of dislocations as the grain size increases. Some studies have reported that subgrain boundaries (*i.e.* boundaries smaller than 15°) may also contribute to Hall-Petch strengthening.²⁰
- *Less efficient solid solution strengthening.* Solute atoms also act as obstacles for the motion of dislocations and grain boundaries. Depending on the atom size, the solute concentration and the type of distortion that they produce, solute atoms may offer weak or strong resistance. At high temperatures, however, both dislocations and grain boundaries can overcome these obstacles more easily.

Fire-resistant steels make use of different approaches, based on their chemical composition, to keep the strength level, σ_y in equation (1), sufficiently high at elevated temperatures. Some steels, for instance, will simply resist the effect of a fire by being thermally stable, which is attained by adding

specific elements in solid solution and increasing σ_{ss} . Others, by contrast, will provide additional strength if precipitation occurs under such extreme conditions, by instantaneously increasing σ_{ppt} . Generally, in fire-resistant steels:

- the dislocation density is kept low to avoid abrupt changes in strength at high temperatures,
- the addition of ferrite stabilizers is used to raise the temperature at which ferrite starts to transform to (soft, coarse-grained) austenite,
- elements in solid solution that produce large atomic misfit strains (strong obstacles) are preferentially employed and,
- nanometer-sized precipitates, which are slow to coarsen, are desirable.

Table 10.1 lists the chemical compositions of two commercial fire-resistant steels, containing Mo and Nb-Mo additions, respectively, manufactured by Nippon steel. The Mo steel in Table 10.1 is designed to simply withstand a fire using the effect of Mo in solid solution, whereas the Nb-Mo steel increases its strength at high temperature by combining the Mo effect with Nb nano-precipitation. It has been observed that with the latter combination, it is possible to reach failure temperatures up to 650°C for the case in which half of the room temperature yield stress is required.²¹ A more recent study has investigated the fire-resistance properties of Fe-C-Mn-Nb steels with no Mo additions.²² In this work, the C-Mn-Nb specimens are soaked at 1100°C for 45 min, rapidly cooled to 850°C and at three different cooling rates, 0.17, 1 and 100°C/s, in the temperature range from 850°C to 600°C, to be finally quenched to room temperature. Afterwards, the specimens are subjected to a standard fire test ISO 834. A reference C-Mn steel is also used for comparison purposes. The obtained results are summarized in Fig. 10.2, which clearly illustrates the contribution of Nb to the failure temperature increase. By addition of 0.1 wt.% Nb to a plain C-Mn steel with no precipitation ($n_{NbC} = 0$), the failure temperature measured during the fire test increases by 92°C. This temperature increment is related to the increase in number density of NbC precipitates, from 0 in the C-Mn steel to 10^{23} m^{-3} in the Nb-microalloyed steel after the fire test. Figure 10.2 also shows that this temperature can be further raised, by 45°C, if besides NbC-precipitation, the density of grain boundaries is increased (*i.e.*, σ_{gb} in equation (1)). It should be noted that the 45°C increment is reached for the fastest cooling rate of 100°C/s due to an increase in the density of both Low (LAGBs) and High (HAGBs) Angle Grain boundaries. The grain boundary density in the Nb-microalloyed steel changes from 0.06 to 0.64 μm^{-1}

Table 10.1: Chemical Composition in wt.% of Two Commercial Fire-resistant Steels Produced by Nippon Steel.²³

Steel	C	Mn	Si	Mo	Nb	S	P
Mo	0.1	0.64	0.1	0.51	—	0.05	0.009
Nb-Mo	0.11	1.14	0.24	0.52	0.03	0.02	0.009

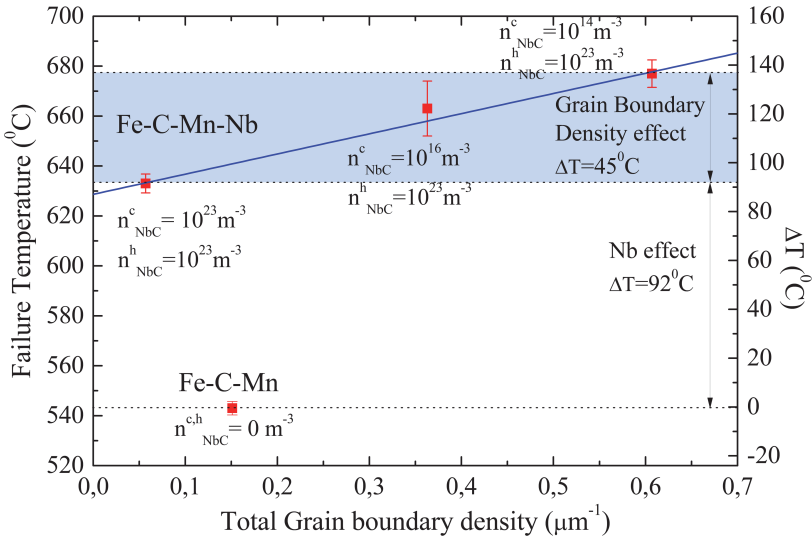


Fig. 10.2. Failure temperature and difference in failure temperature with respect to a reference material (Fe-C-Mn) as measured during a standard fire test ISO 834 as a function of the total grain boundary density for a C-Mn-Nb alloy. The number density of NbC precipitates calculated before (n_{NbC}^c) and after (n_{NbC}^h) the fire test are also indicated.²² Reprinted from 'Scripta Materialia', vol. 68, E. Gözde Dere, Hemant Sharma, Roumen H. Petrov, Jilt Sietsma and S. Erik Offerman, 'Effect of niobium and grain boundary density on the fire resistance of Fe-C-Mn steel', Pages 651–654, 2013, with permission from Elsevier.

by increasing the cooling rate during the $\gamma \rightarrow \alpha$ phase transformation from $0.17^{\circ}\text{C}/\text{s}$ to $100^{\circ}\text{C}/\text{s}$.

10.2.2 Chassis and suspension systems

The chassis and suspension are the most important components of a car in order to maintain driving stability, and thus, their high reliability is indispensable. Similar to other parts of the car, weight targets also extend to the automotive chassis system and promote the use of stronger materials

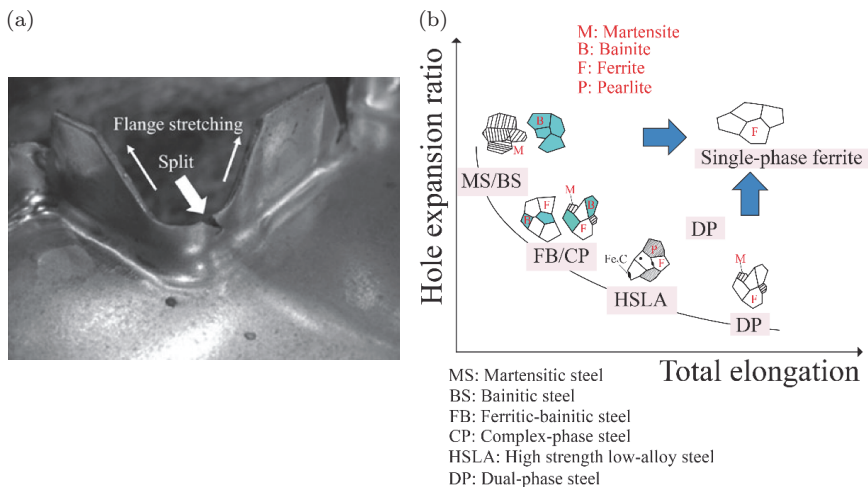


Fig. 10.3. (a) Crack initiation at a sheared edge of a component made from DP780 after flanging.²⁵ Reprinted with permission from Springer, in *Advances in Manufacturing*, 'Reverse metallurgical engineering towards sustainable manufacturing of vehicles using Nb and Mo alloyed high performance steels, Hardy Mohrbacher, 2013. (b) Microstructure effect on the balance between elongation and hole expansion ratio.

for these applications. Yet, chassis designs require very complex shapes that are only obtained after several forming processes are applied, including blanking, punching, stretch-flanging, and hole expansion operations. These processes are often limited by the strength of the steel and the presence of hard phases, particularly martensite, that are inhomogeneously distributed within the steel microstructure. Steels with several phases are not suitable for these applications,²⁴ as usually voids and cracks are generated during forming by decohesion of hard phase-soft phase interfaces.

Currently, and despite their limitations, AHSS such as ferrite-bainite (FB) and/or dual-phase (DP) steels are adopted for these high-tech applications. The shortcomings are clearly illustrated in Fig. 10.3. Figure 10.3(a) shows a common problem of edge splitting during flanging operations when using a DP steel,²⁵ whilst Figure 10.3(b) schematically displays the balance between the hole expansion ratio and the total elongation for different AHSS microstructures. The latter demonstrates that single-phase AHSS, that is, martensitic (MS) and bainitic (BS) steels, exhibit high hole expansion ratio, but poor elongation. DP steels, conversely, display high elongation, though the capacity for hole expansion ratio is very limited. Somewhere in between lie the FB, complex-phase (CP) and HSLA steels. Figure 10.3 shows the

necessity for the development of steels that, besides having a good strength-ductility balance, are also suitable for demanding forming operations. As shown in Fig. 10.3(b), the appropriate steel must adopt a single phase ferrite structure to reach the hole expansion ratio of bainitic/martensitic steels, and at the same time, keep the elongation high. Other desired properties are also high yield and tensile strengths, good bendability, fatigue strength, and weldability. The strength of the steel is maximized by grain refinement, precipitation strengthening, and by using thermally stable nanometer-sized precipitates (to avoid coarsening and the subsequent loss in strength during steel processing). This new type of AHSS described here is the promising nano-steel.

It has been observed, for instance, that in nano-steels containing Ti and Mo additions, tensile strengths of 780 MPa can be reached when the Ti/Mo atomic ratio is 1. In that case, very fine carbides (3 nm) aligned in rows (*i.e.*, interphase precipitation) have been noticed.¹¹ The strengthening contribution from these extremely fine precipitates exceeds by far the amount of conventional precipitation strengthening achieved to date in HSLA steels. Figure 10.4 shows the decrease in strength experienced during isothermal annealing at 650°C by two different steels, a conventional HSLA

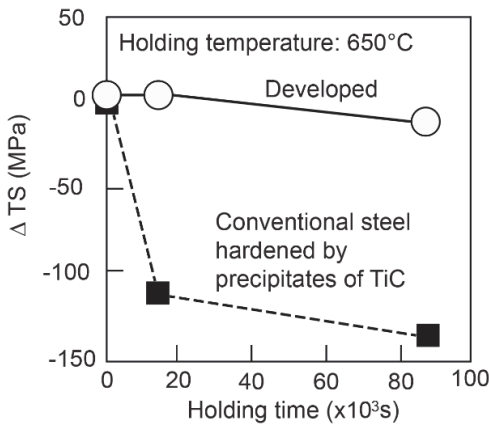


Fig. 10.4. Loss in strength undergone by a conventional HSLA steel (black squares) and a nano-steel based on Ti additions (white circles) during isothermal annealing at 650°C.²⁶ Reprinted by permission of Taylor & Francis Ltd (<http://www.tandfonline.com>) on behalf of Institute of Materials, Minerals and Mining, article title: 'Application of nanoengineering to research and development and production of high strength steel sheets', by K. Seto & H. Matsuda, Materials Science and Technology, copyright © (2013) Institute of Materials, Minerals and Mining.

steel microalloyed with Ti and a nano-steel containing Ti and Mo additions. The former is hardened with TiC-precipitation and the latter with (Ti,Mo)C precipitates that have a smaller size distribution.²⁶ It can be seen in Fig. 10.4 that the tensile strength TS of the nano-steel remains practically the same after annealing for very long times, whereas it abruptly decreases at 15000 s for the conventional HSLA steel, caused by faster TiC coarsening. The precipitates in the HSLA steel are bigger and thus more prone to grow. The results in Fig. 10.4 confirm the remarkably higher stability of (Ti,Mo)C-precipitates in the nano-steel. It has been reported that Mo accelerates the nucleation stage and reduces the precipitate size by reducing the interfacial energy between the precipitate and the matrix (i.e., the lattice misfit).^{27,28} Nevertheless, Mo is not thermodynamically favored within the precipitate and subsequent stages of growth and coarsening require that it partitions to the matrix, so that these latter stages are consequently delayed.

Combinations of Nb and Mo additions, either alone or together with Ti, are also being investigated.^{25,27,29} One of the advantages of Nb microalloying is the austenite pancaking during hot rolling that promotes finer ferritic microstructures. Fast cooling from the finish rolling temperature to the temperature range of ferrite formation and subsequent (Ti,Nb,Mo)C interphase precipitation during phase transformation, delayed by solute Nb, is the main processing strategy behind this type of steel. As observed in Fig. 10.5, this new alloy concept, using a combination of 0.04wt.%C-1.4wt.%Mn-0.09wt.%Nb, exhibits excellent bendability and high quality cutting edges, but also high hole expansion ratio and elongation.²⁵

10.3 Mechanisms of Precipitation Strengthening

In order to better understand the large precipitation strengthening contribution σ_{ppt} generally obtained in nano-steels, essential for fire-resistance and chassis applications, the current section focuses on the main mechanisms by which precipitates might strengthen the steel. In general, precipitation strengthening in micro-alloyed steels arises primarily from the interaction of the moving dislocations and the precipitates, namely from:

- stress fields generated around precipitates, due to a slight misfit between the precipitates and the matrix, which hinders the motion of dislocations as depicted in Fig. 10.6, known as *coherency strengthening* (σ_{coh}),
- dislocations cutting coherent precipitates and creating both an additional precipitate/matrix interface, designated as *chemical strengthening* (σ_s),

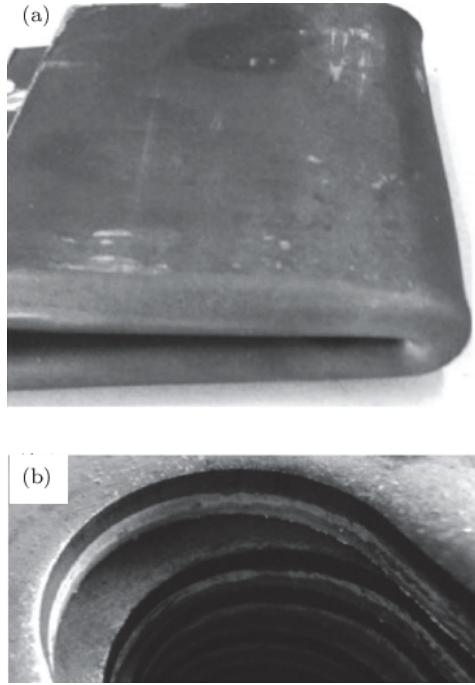


Fig. 10.5. Bendability and hole punching properties of a 0.04wt.%C-1.4wt.%Mn-0.09wt.%Nb steel.²⁵ Reprinted by permission from Springer, in *Advances in Manufacturing*, ‘Reverse metallurgical engineering towards sustainable manufacturing of vehicles using Nb and Mo alloyed high performance steels, Hardy Mohrbacher, 2013.

and an anti-phase boundary, referred to as *order strengthening* (σ_{APB}) illustrated in Fig. 10.8, and

- dislocations looping around incoherent precipitates, see Fig. 10.9, which is called *dispersion strengthening* (σ_D), shown in Fig. 10.10.

Note that a precipitate is coherent if it matches perfectly with the atomic structure of the matrix at the interface (see Fig. 10.7). Thus, coherent precipitates provide continuity of slip planes between the matrix and the precipitates and are shearable. For small coherent precipitates, the coherency strengthening is given by³⁰:

$$\sigma_{coh} = 4.1MG\varepsilon^{3/2}f^{1/2}\left(\frac{r}{b}\right)^{1/2} \quad (2)$$

where M is the Taylor factor, G is the shear modulus, ε is the misfit of the precipitate, f is the volume fraction of precipitates, b is

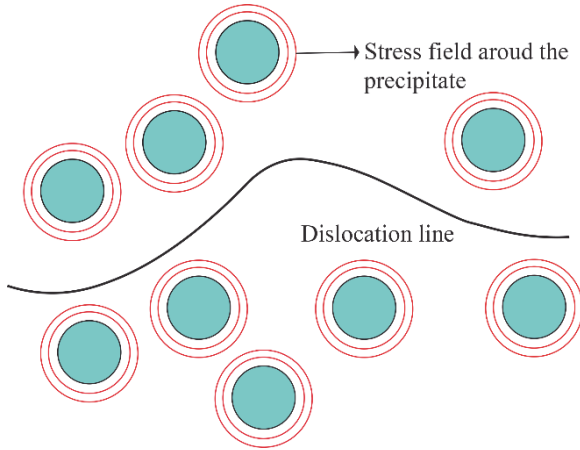


Fig. 10.6. Interaction between a dislocation and the stress field of the precipitates.

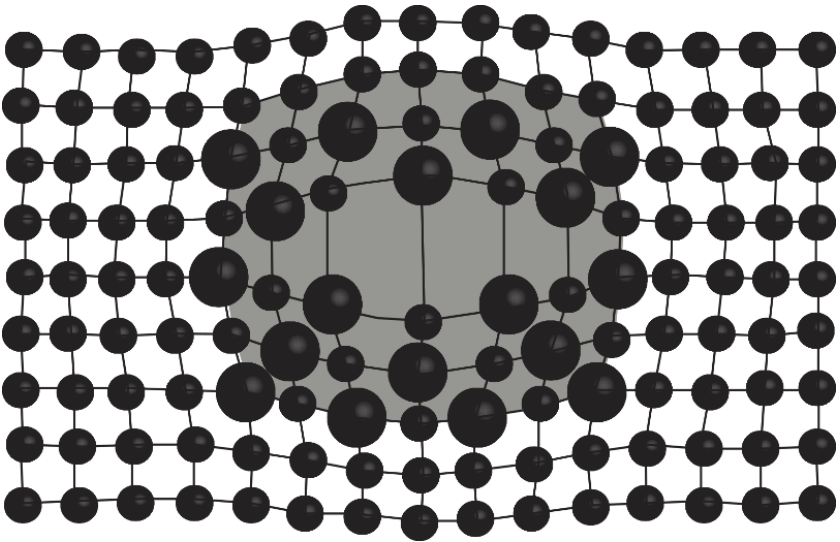


Fig. 10.7. Schematic representation of a coherent precipitate with large strain fields.

the magnitude of the Burgers vector and r is the average precipitate radius. For larger coherent precipitates, the following equation is used instead³⁰:

$$\sigma_{coh} = 0.7MG\varepsilon^{1/4}f^{1/2}\left(\frac{b}{r}\right)^{3/4} \quad (3)$$

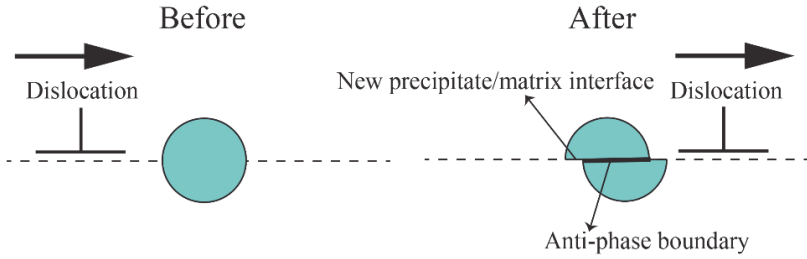


Fig. 10.8. A dislocation cutting through a precipitate coherent with the matrix.

The chemical strengthening can be estimated as³¹:

$$\sigma_s = 2MG \left(\frac{3}{\pi} \right)^{1/2} \left(\frac{\gamma_s}{Gb} \right)^{3/2} \left(\frac{b}{r} \right) f^{1/2} \quad (4)$$

in which γ_s is the energy of the precipitate-matrix interface. Usually γ_s is smaller than the energy necessary to create an antiphase boundary γ_{APB} and the chemical strengthening does not contribute significantly to increase the strength of aged alloys. If an antiphase boundary, *i.e.* a region where the order of the precipitate is disrupted (see Fig. 10.8) is created inside the particle with ordered structure, restoration of the precipitate order requires the dislocations to glide in pairs: the first dislocation creates an antiphase boundary, whereas the second returns the order. This leads to a strengthening increase given by³²:

$$\sigma_{APB} = M \frac{\gamma_{APB}}{2b^2} \left(\left(\frac{3\pi^2 \gamma_{APB} f r}{32T} \right)^{1/2} - f \right) \quad (5)$$

where T is the line tension of the dislocation.

Conversely, a precipitate is incoherent if the interface plane has a very different atomic configuration in the matrix and the precipitate. This implies that incoherent precipitates cannot be cut by dislocations nor deformed with the matrix. Figure 10.9 displays a schematic illustration of an incoherent precipitate.

There are three different possibilities by which the dislocations can then overcome incoherent precipitates: (1) looping around the precipitate, also known as the Orowan mechanism, leaving a dislocation loop behind, (2) climbing and (3) cross-slipping. Although dislocation release at higher stresses can also occur by cross-slip, the latter two mechanisms acquire more relevance at high temperature. In precipitation strengthening by the Orowan mechanism, it is assumed that the precipitates are hard, do not

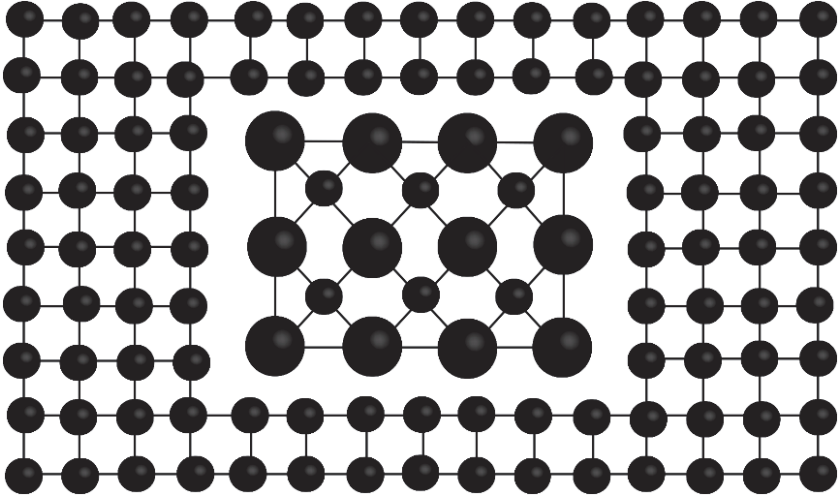


Fig. 10.9. Schematic representation of an incoherent precipitate.

deform with the matrix and act as pinning points for dislocations. Considering the line tension of a dislocation, *i.e.* the force in the direction of the line vector that tries to shorten the dislocation, is $\sim \frac{Gb^2}{2}$, the stress necessary to bypass the precipitate can be estimated from the balance of forces between the particle resistance to dislocation motion and the line tension of dislocation as (see Fig. 10.10):

$$\sigma_D = \frac{MGb}{L} \tag{6}$$

where L is the average precipitate spacing. It should be pointed out, however, that this equation overestimates the real stress required to bypass a particle and usually represents an upper bound.³³ More accurate is the equation given by Ashby-Orowan that considers the effects of statistically distributed particles.³³ The latter is suitable for the cases in which the particle size is negligible with respect to the particle spacing. Taking into account the effect of self-interaction between dislocation lines on each side of the particle, the Ashby-Orowan equation can be expressed as¹⁹:

$$\sigma_D = \frac{kMGb}{2\pi\sqrt{1-\nu}L} \ln\left(\frac{x}{2b}\right) \tag{7}$$

in which k is a factor of 0.8, accounting for heterogeneity in particle distribution, ν is the Poisson's ratio, $\sqrt{1-\nu}$ is introduced as an average of the energy difference between screw and edge characters and x is the average

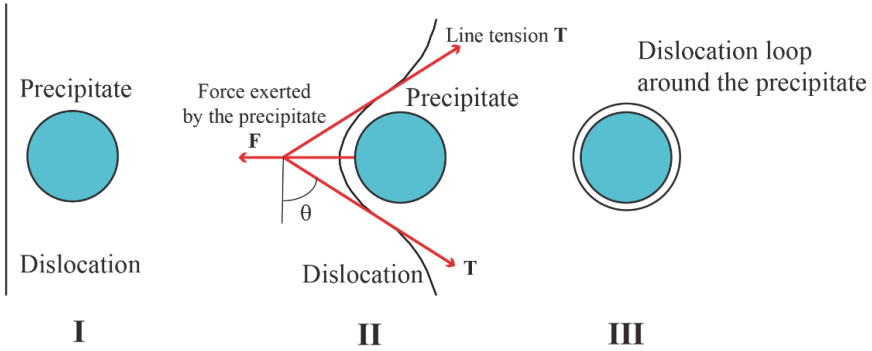


Fig. 10.10. Dislocation bypassing an obstacle by the Orowan mechanism.

diameter of the precipitates on the slip plane. For precipitates randomly distributed in the matrix^{19,34}:

$$L = \sqrt{\frac{2}{3}} \left(\sqrt{\frac{\pi}{f}} - 2 \right) \cdot r \quad (8)$$

and

$$x = 2\sqrt{\frac{2}{3}} r \quad (9)$$

Equations (8) and (9) are valid if interphase precipitation does not occur that is, for random precipitation, or in case it does, if the sheet spacing is larger and/or comparable to the particle spacing. If, by contrast, the sheet spacing is smaller, the interphase-precipitated particles cannot be considered randomly distributed and equations (8) and (9) are no longer applicable. In this particular case, L can be calculated as³⁵:

$$L = \sqrt{r_1 r_2} \quad (10)$$

where r_1 is the mean linear inter-particle spacing along the intersection between the slip plane and the sheet plane of interphase precipitation and r_2 is the mean projected value of the perpendicular sheet spacing. r_1 and r_2 can be determined through the measured particle spacing ω , the sheet spacing, the particle aspect ratio p and the particle radius r as³⁵:

$$r_1 = \frac{\omega^2}{2r} + \frac{\pi r}{2} - \frac{2r}{p \sin \theta} \quad (11)$$

$$r_2 = \frac{\lambda - 2r \sin \theta}{\sin \varphi} \quad (12)$$

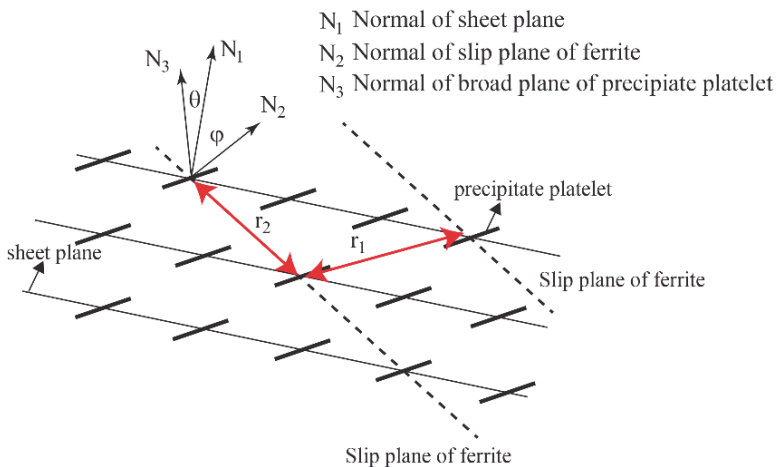


Fig. 10.11. Schematic representation of the geometric orientation between the sheet plane, the carbide platelets and the ferrite slip plane as in³⁵. Reprinted from Acta Materialia, Vol. 64, M.-Y. Chen, M. Gouné, M. Verdier, Y. Bréchet, J.-R. Yang, Interphase precipitation in vanadium-alloyed steels: Strengthening contribution and morphological variability with austenite to ferrite transformation, Pages 78–92, Copyright 2014, with permission from Elsevier.

in which θ is the angle between the precipitate broad plane normal and the sheet plane normal, and φ is the angle between the sheet plane normal and the slip plane normal. The geometric orientation between the sheet plane, the precipitates and slip plane are depicted in Fig. 10.6.

Precipitation strengthening involves a complex series of physical transformations that induce different strengthening mechanisms over time. In many cases, these transformations occur at such small scale that it is very difficult and tricky to identify the underlying mechanisms, giving rise to a controversy among researchers. A good example of this is the debate generated around the early stages of precipitation in microalloyed steels, for which no theory has been generally accepted so far. Several precipitate nucleation processes have been observed in microalloyed steels and these include homogeneous (uniformly and non-preferentially), interphase and heterogeneous (preferentially at specific sites such as dislocations, grain boundaries and/or vacancies) precipitation. It has been proposed that homogeneous precipitation in microalloyed steels follows the sequence Guinier-Preston (GP) zones \rightarrow intermediate phase \rightarrow equilibrium phase seen in non-ferrous alloys.³⁶ This sequence is schematically illustrated in Fig. 10.12 and can be explained as follows. During a first stage, solute-rich

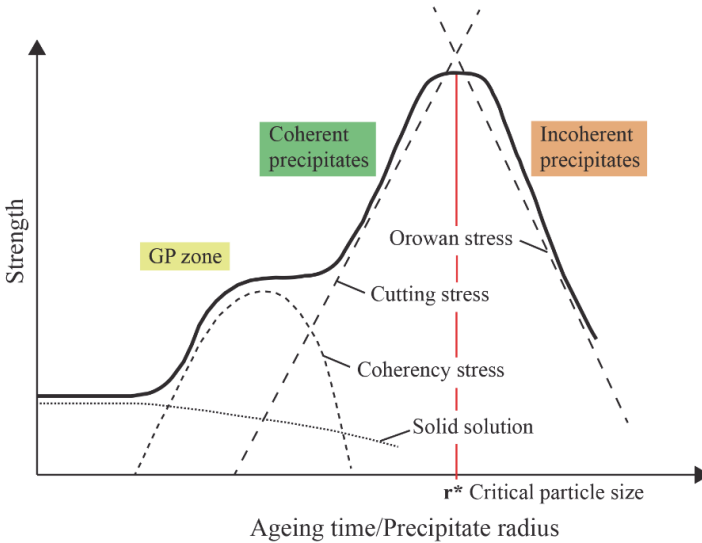


Fig. 10.12. Schematic illustration of the precipitate strengthening contributions.

clusters (also called GP zones) are formed within the lattice driven by the high concentration of alloying elements in solid solution, which exceeds the equilibrium solubility limit. Atomic diffusion and clustering of the alloying elements is assisted by vacancies in the lattice. These solute-rich GP zones are coherent with the steel matrix and the atomic structure is continuous across the interface. In the next step, the GP zones transform into small coherent precipitates which distort the surrounding matrix due to their misfit and produce stress fields that impede dislocation motion (*coherency strengthening*). Once the dislocation has overcome these stress fields and reached the precipitate, it can pass through the particle, provided it surmounts the particle resistance (*chemical and order strengthening*), since the slip planes are coherent with the matrix. Eventually, coherent precipitates transform into incoherent ones as they grow, changing their crystal structure so that the atomic structure between the precipitate and the matrix is no longer continuous. Incoherent precipitates are distinct second-phase particles, with their own crystal structure and separated from the matrix by well-defined interfaces. Incoherent precipitates are more effective obstacles against dislocation motion (*dispersion strengthening*) and the only manner to overcome these obstacles is the dislocation bowing-out and looping around the precipitates. The maximum strengthening is attained at the moment coherent precipitates transform into incoherent

ones. As soon as the latter grow slightly, the strengthening effect decreases. It should be emphasized, though, that even in that case the Orowan mechanism contributes to strength increase if compared to the condition of non-precipitation.

Regarding the nucleation stage, there is practically no reason for coherent precipitates to form in the stress field of a dislocation, essentially because the precipitate and the matrix lattices already match. Similarly, it is very unlikely that these precipitates nucleate at the grain boundaries. Only in the case of coherent precipitates with large elastic strains, for example when the precipitate nucleus is significantly larger than that of the matrix, is nucleation on vacancies favored. Semi-coherent precipitates, containing interfacial dislocations to relax the coherency strains, will nucleate much easier on dislocations. Incoherent precipitates, by contrast, with little or no atomic matching across the precipitate-matrix interface, will preferentially nucleate at the grain boundaries. As the size of coherent precipitates increases, coherent precipitates will transform into incoherent ones, which produce less lattice distortion, but have higher energy and mobility, and hence, grow faster. This means that at high temperatures incoherent precipitates will coarsen faster than coherent precipitates. Yet, coherent precipitates provide less resistance to dislocation motion. A balance between these two features can be accomplished by coherent precipitates with large strain fields.

10.4 Potential for Alternative Microalloying Elements: Replacing Nb by V.

10.4.1 *Precipitation strengthening in V-microalloyed steels*

Vanadium (V) has been used in steels as a microalloying element during the last decades, and the reason for this is that it has a great potential for ferrite strengthening. It forms nitrides (VN), carbonitrides (V(C,N)) and/or carbides (VC), depending on the temperature range and the steel's chemical composition. The solubility of these species increases in the abovementioned order, which means that VC and VN are the most and the least soluble particles, respectively. Moreover, this solubility is significantly smaller in ferrite than in austenite. Comparing to other microalloying elements that also form nitrides and carbides, like Ti, Nb and Al (Al only forms nitrides), V is the most soluble element and does not readily precipitate in austenite. Thus, although VN and V(C,N) can additionally be used for ferrite grain refinement, either by delaying austenite recrystallisation kinetics or by

providing intragranular ferrite nucleation sites,^{37–40} the primary objective of V addition in steel is V(C,N) or VC-precipitation strengthening. The latter usually occurs in ferrite during or after the $\gamma \rightarrow \alpha$ phase transformation upon cooling and coiling. Furthermore, the V-precipitation strengthening contribution can be enhanced by N addition, that is, at a given vanadium content, vanadium provides more strengthening when combined with N, up to the stoichiometric V:N.⁴¹ Increasing the N content increases the driving force for V-precipitation, resulting in a smaller particle size, smaller inter-particle spacing and a greater resistance to coarsening.⁴² Earlier work shows that additions of V and N significantly increase the yield stress.⁴³

At relatively high temperatures in the austenitic regime, when the driving force for precipitation is small, V(C,N)-precipitates nucleate heterogeneously on dislocations and/or grain boundaries. These precipitates will lose coherency and be incoherent with the ferrite matrix afterwards. At lower temperatures, in the intercritical ($\gamma + \alpha$) regime, V(C,N) interphase precipitation occurs during the $\gamma \rightarrow \alpha$ phase transformation. In this case, the precipitates nucleate at the migrating γ/α interface and form periodic arrays of sheets parallel to the transformation front. Note that because interphase precipitates are randomly arranged within the sheets, depending on the sheet orientation with respect to the observation plane, precipitates may appear as either well-defined lines or randomly distributed particles. Besides this, random interphase precipitation may also take place. Whether interphase precipitation occurs in sheet-like form or randomly depends on the crystallographic characteristics of the interface between the parent austenite and the ferrite.⁴⁴ For instance, it has been observed that V(C,N) interphase precipitation is suppressed when the γ/α orientation relationship is close to the Kurdjumov-Sachs orientation relationship (K-S, $(111)_{\gamma\text{-Fe}} \parallel (011)_{\alpha\text{-Fe}} \parallel [\bar{1}01]_{\gamma\text{-Fe}} \parallel [\bar{1}\bar{1}1]_{\alpha\text{-Fe}}$ [44]). It has been claimed that interphase V(C,N)-precipitates in commercial V-microalloyed steels, despite being incoherent with the ferrite matrix, follow a single variant of the Baker-Nutting (B-N) orientation relationship $(100)_{\alpha\text{-Fe}} \parallel (100)_{\text{VC}} \parallel [011]_{\alpha\text{-Fe}} \parallel [010]_{\text{VC}}$.⁴⁵ Some authors have observed using Atom Probe Tomography (APT) that these precipitates consist of C, Mn and V,⁴⁶ whilst others have reported that Mn is homogeneously distributed within the matrix.⁴⁷ Additionally, it has been shown that finer interphase V(C,N)-precipitates can be obtained by reducing the transformation temperature and increasing the V content, whereas the bulk C content hardly affects the particle size [47]. At these or even lower temperatures, homogeneous precipitation from supersaturated ferrite can also occur. It has been proposed that these

V(C,N)-precipitates have a coherent particle-ferrite matrix interface at the early stages of precipitation, which becomes semi-coherent and subsequently incoherent during growth.⁴⁸ Although, in principle, this agrees well with the lattice mismatch calculated for different carbonitrides in ferrite, according to which V(C,N) particles have the smallest misfit, and thus need larger sizes to lose coherency,^{36,45} this hypothesis is still debatable at the present time. The controversy arises mainly from the difficulties in TEM observation and the distinction of strain field contrasts exclusively related to V(C,N) and not to any other artefact. According to ref. [46], homogeneously precipitated V(C,N) particles might have a different chemical composition from interphase precipitates. In any case, they also follow an orientation relationship of the Baker-Nutting (B-N) type, being in this case the three feasible variants possible.³⁶ It is clear from the above that further work is still necessary in this regard, as the distinction between coherent and incoherent precipitates is fundamental in order to estimate the real strengthening contribution of V(C,N) particles (see previous section).

10.4.2 *Is Vanadium addition the best approach?*

Vanadium is a promising candidate to (partially) replace Nb and Ti in nano-steels. It is a ferrite stabilizer element and as explained before, its higher solubility is a great advantage: while most of the V remains in solid solution in austenite and only precipitates during or after $\gamma \rightarrow \alpha$ phase transformation, other microalloying elements, such as Ti and/or Nb, precipitate at higher temperatures and are less effective at providing precipitation strengthening in ferrite. Small additions of Ti and Nb are beneficial to avoid grain coarsening during soaking in the reheating furnace and prevent austenite recrystallisation during thermomechanical processing. However, by the time the austenite starts to transform into ferrite in Ti,Nb-microalloyed steels, a significant quantity of TiC and/or NbC particles have already formed. These particles will be incoherent with the ferrite matrix and relatively large, providing limited dispersion hardening according to equations (6) and (7) and coarsening fast. It should be pointed out that V can be combined with N to further enhance precipitation hardening: for a given transformation temperature, the sheet spacing as well as the particle size of VN and V(C,N)-precipitates is smaller than that of the VC. This is not the case for Ti-,Nb-microalloyed steels, since the corresponding carbonitrides will form in austenite at even higher temperatures. Also, it should be borne

in mind that when Ti is combined with V and N, to ensure a relatively fine austenite grain size, Ti is a strong nitride former and will react first with N to form TiN. This implies that less N will be available for later precipitation with V. Although high N V-microalloyed steels have sometimes been considered inadequate for welding, recent studies have shown that these steels are compatible with weldability by an appropriate choice of the microalloying additions and welding parameters.³⁶

The precipitates in nano-steels should be thermally stable, which is particularly important for fire-resistant steels, and at the same time, effective in hindering the motion of dislocations. It has been seen in section 3 that coherent precipitates with large strain fields are the best approach to attain these two properties simultaneously. A very important point to consider, though, is that coherence strain fields associated with nitrides, carbides and carbonitrides have rarely been reported in the literature for microalloyed steels, other than V(C,N)-precipitates.⁴⁸ Hence, the latter seem preferable for these new types of steels. Ti- and Nb-based nano-steels usually make use of Mo additions to keep the precipitates small and increase their thermal stability. So far, there is no information available in the literature regarding the interaction of Mo and V in (Mo,V)(C,N)-precipitates. The question to answer now is whether or not the combination of V, N and Mo results in even better nano-steels, which, besides being “resource efficient”, are satisfactory for high standard applications.

It has been seen that VC nanometer-sized carbides can significantly improve the mechanical properties of a conventional ferritic steel. Their contribution to the steel strength can be estimated by the Ashby-Orowan model (equations (7)–(12)). Kamikawa *et al.* have reported, for instance, yield and ultimate tensile strengths of 640 MPa and 830 MPa, respectively, in a low carbon steel with 0.1wt.%C, 0.22wt.%Si, 0.83wt.%Mn and 0.288wt.%V, after being austenitised at 1200°C for 10 min and isothermally transformed at 690°C for 300 s.¹⁹ Moreover, the measured uniform and total elongation are relatively high, viz. 10% and 20%, respectively. VC-precipitates of 4.5 nm diameter are the reason behind this substantial improvement. The precipitation strengthening contribution (σ_{ppt} in equation (1) calculated by equations (7), (8), and (9)) yields for this particular case 385 MPa. However, it should be pointed out that this value decreases to 200 MPa as the isothermal holding time at 690°C is increased from 300 s to 48 h, caused by VC-precipitate coarsening. Chen *et al.* have observed that a given V(C,N) volume fraction, the precipitation strengthening associated with interphase precipitation, calculated by means of equations (6), (10), (11) and (12), may vary between 100 MPa and 300 MPa, depending on the particle size and

arrangement, *i.e.* sheet spacing and inter-particle spacing.³⁵ Similarly, other authors have reported precipitation strengthening contributions of both interphase and random (V,Ti)C precipitates of 300 MPa.⁴⁹ Due to their beneficial effect, it has also been proposed that V(C,N)-precipitates can be used to develop “nano-precipitated DP steels”,⁵⁰ containing ferrite, martensite and a dispersion of very fine V(C,N) precipitates in ferrite. Mechanical experiments conducted on these microstructures have shown that V(C,N) nano-precipitation significantly increases the strength of DP steels, with almost no loss in ductility when the ferrite fraction is $\leq 50\%$. Besides, precipitation strengthening notoriously improves the strength-ductility balance. Strain partitioning between the ferrite and the martensite is suppressed by the fine dispersion of precipitates, which also act as sources for dislocation multiplication.

10.4.3 Industrial implications

The desirable properties of nano-steels are attained basically through ferrite grain refinement and nanometer-sized precipitates of the corresponding carbonitrides. Industrial and commercial implementation of these steels requires the maximization of these two effects at the lowest cost. For Nb-microalloyed steels, usually controlled rolling (CR) is used as thermomechanical processing, including two well-differentiated stages: deformation at high temperatures in the recrystallisation region and deformation below the stop recrystallisation temperature. The latter produces a deformed austenite microstructure prior to phase transformation and enhances ferrite nucleation at deformation bands in the austenite grain interior, providing additional ferrite grain refinement. However, powerful mills are necessary under these conditions because of the steel's high resistance to deformation. Moreover, deformed austenite is not the only approach to obtain a fine ferrite microstructure in the later processing stages.⁵¹ In the case of V-microalloyed steels, most of the V remains in solid solution in this temperature regime, which allows the use of recrystallisation controlled rolling (RCR) as thermomechanical processing. The latter is, conversely, not suitable for Nb-microalloyed steels. As an advantage to CR, higher finish rolling temperatures can be employed in RCR to reduce the roll force requirements. Accelerated cooling combined with lower cooling temperatures after RCR and V(C,N) nano-precipitation might be an appropriate strategy to reach the high-standard requirements.^{51,52} The accelerated cooling contributes to ferrite grain refinement (increases σ_{gb} in equation (1)) and can be used to compensate for the larger austenite grain sizes obtained after soaking, in the

absence of other microalloying elements, and when the finish rolling temperature is increased. In addition, the use of V as a microalloying element has other benefits if compared to Nb: excellent castability with minimal cracking, reduced reheating/soaking requirements, and predictable strengthening over a large alloy range. Low ductility in microalloyed steels is attributed to strain-induced precipitation of carbonitrides at the austenite grain boundaries. The limited strain-induced precipitation of V(C,N) makes V less detrimental in this regard.⁵³ Also, it should be pointed out that high N levels from electric arc furnaces are no longer a problem in V-microalloyed steels.

The kinetics of the austenite grain growth during soaking can be explained by equation (13) when temperature and time are the main controlling variables⁵⁴:

$$D^2 - D_0^2 = K \exp\left(-\frac{Q}{RT}\right) \tau \quad (13)$$

in which D_0 and D are the mean austenite grain sizes at times τ_0 and τ , respectively, K is a constant, Q is the activation energy for grain growth, R is the gas constant, and T is the temperature. Austenite grain size is usually controlled during soaking by small additions of Ti and/or Nb, which are also strong nitrides and carbides formers and have smaller solubility than V in austenite. Higher temperatures than that of soaking are necessary in CR and RCR to dissolve the latter precipitates, which thus prevent grain coarsening. On the other hand, non-dissolved VN and/or V(C,N) precipitates can also be effective in controlling the austenite grain size at lower temperatures, in warm working conditions such as those applied in warm forging, where the soaking temperature is usually low (e.g., below 900°C).⁵⁴ By studying the kinetics of austenite grain growth in three different steels, with chemical compositions (in wt.%) 0.4C-1Mn-0.004N, 0.4C-1Mn-0.04N and 0.4C-1Mn-0.04N-0.078V, Staško *et al.* have shown that undissolved V(C,N) particles inhibit austenite grain growth effectively, keeping the grain size small (~ 5.45 – $8.1 \mu\text{m}$) in the range of temperatures between 840–1000°C. In the temperature range of 1050–1200°C, by contrast, austenite grain growth occurs due to the complete dissolution of these precipitates. Indeed, in the latter case, the N dissolved in the austenitic matrix promotes grain growth by reducing the activation energy for grain boundary migration. It is suggested in that work that interstitial elements, such as N and C, dissolved in austenite reduce the binding energy between Fe atoms in the matrix favoring the austenite grain growth in the absence of precipitates. Similar

results have been found by Adamczyk *et al.* for two steels with chemical compositions (in wt.%) 0.27C-1.4Mn-0.35Si-0.2V-0.025Al-0.016N and 0.25C-1.4Mn-0.33Si-0.15V-0.011Al-0.018N. They have seen in their work that V(C,N) and AlN particles hinders the austenite grain growth in the two steels up to 1000°C. Above this temperature, the density of undissolved precipitates is small and precipitate coarsening occurs, causing rapid austenite grain growth.

The effect of V in hot working conditions has largely been studied.^{55,56} It is well-known that the effect of V solute drag on the static recrystallisation kinetics, caused by V in solid solution, is small compared to that of Nb. This effect has been quantified by the so-called solute retardation parameter (SRP), which quantifies the delay observed in recrystallisation time by the addition of 0.1 wt.% of a microalloying element (e.g. Nb, Ti, Mo or V) to a C-Mn base steel. It has been shown that $SRP(Nb)=222$, whereas $SRP(V)=13$.⁵⁷ By contrast, although less effective than Nb(C,N), precipitation of V(C,N) particles on dislocations (strain-induced precipitation) has also been shown to affect the static recrystallisation kinetics of austenite, mainly in the low temperature regime.³⁷ Moreover, depending on the soaking temperature, which will define the amount of undissolved precipitates, V can also delay the austenite recrystallisation kinetics by non-dissolved V(C,N). In contrast to strain-induced V(C,N) precipitation, undissolved V(C,N) particles are already present before deformation and cannot stop recrystallisation completely. Yet, they effectively delay static recrystallisation at low temperatures corresponding to warm working conditions⁵⁸. Both strain-induced and undissolved V(C,N) can act as nucleation sites for the formation of intragranular ferrite in later stages, contributing to a significant ferrite grain refinement.^{38,39}

References

1. European Commission. (2011). *A resource efficient Europe — flagship initiative under the Europe 2020 strategy*. Brussels, Belgium: European Commission.
2. European Commission. (2013). *Action plan for a competitive and sustainable steel industry in Europe*. Brussels, Belgium: European Commission.
3. Allwood, J. and Cullen, J. (2012). *Sustainable materials — with both eyes open*. Cambridge, UK: Cambridge Institute for Sustainability Leadership.
4. Rijkenberg, R.A. and Hanlon, D.N. (2013). *WO2013167572A1*. Automotive chassis part made from high strength formable hot rolled steel sheet. Tata Steel Europe. Geneva, Switzerland: WIPO.

5. Rijkenberg, R.A. (2014). *WO2014122215A1*. A high-strength hot-rolled steel strip or sheet with excellent formability and fatigue performance and a method of manufacturing said steel strip or sheet. Tata Steel Europe. Geneva, Switzerland: WIPO.
6. Funakawa, Y., Shiozaki, T., Tomita, K., Saito, T., Nakata, H., Sato, K., Suwa, M., Yamamoto, T., Murao, Y., and Maeda, E. (2003). *EP1338665A1*. High tensile hot rolled steel sheet and method for production thereof. JFE Steel Corporation. Munich, Germany: EPO.
7. Ariga, T., Nakaajima, K., and Funakawa, Y. (2013). *EP2554705A1*. Hot-dip galvanized steel sheet with high tensile strength and superior processability and method for producing same. JFE Steel Corporation. Munich, Germany: EPO.
8. Kariya, N., Takagi, S., Shimizu, T., Mega, T., Sakata, K., and Takahashi, H. (2006). *EP1616970A1*. High strength hot-rolled steel plate. JFE Steel Corporation. Munich, Germany: EPO.
9. Yokota, T., Kobayashi, A., Seto, K., Hosoya, Y., Heller, T., Hammer, B., Bode, R., and Stich, G. (2007). *EP1790737A1*. A high strength steel excellent in uniform elongation properties and method of manufacturing the same. JFE Steel Corporation and ThyssenKrupp Steel. Munich, Germany: EPO.
10. Kömi, J., Keltamäki, K., Intonen, T., Kinnunen, H., Outinen, J., Porter, D., and Rasmus, T. (2008). *EP2235226A1*. Method for selecting composition of steels and its use. Rautarukki Oyj. Munich, Germany: EPO.
11. Funakawa, Y., Shiozaki, T., Tomita, K., Yamamoto, T., and Maeda, E. (2004). Development of high strength hot-rolled sheet steel consisting of ferrite and nanometer-sized carbides. *ISIJ International*, 44(11), 1945–1951.
12. Lee, W.B., Hong, S.G., Park, C.G., Kim, K.H., and Park, S.H. (2000). Influence of Mo on precipitation hardening in hot rolled HSLA steels containing Nb. *Scripta Materialia*, 43(4), 319–324.
13. Zhang, Z., Yong, Q., Sun, X., Li, Z., Wang, Z., Zhou, S., and Wang, G. (2015). Effect of Mo addition on the precipitation behavior of carbide in Nb-bearing HSLA steel. *HSLA Steels 2015, Microalloying 2015 and Offshore Engineering Steels 2015*. Hangzhou, Zhejiang Province, China: The Chinese Society for Metals and Chinese Academy of Engineering.
14. European Commission. (2014). *On the review of the list of critical raw materials for the EU and the implementation of the Raw Materials Initiative*. Brussels, Belgium: European Commission.
15. Fushimi, M., Chikaraishi, H., and Keira, K. (1995). *Development of fire-resistant steel frame building structures*. Tokyo, Japan: Nippon Steel.
16. Standards Australia. (1985). AS 1530.4. *Fire resistance tests of elements of building construction*. Sydney, Australia: Standards Australia.
17. American Society of Testing Materials. (1996). ASTM E119. *Standard test method for fire tests of building construction and materials*. Philadelphia, PA, USA: American Society of Testing Materials.
18. ECCS Technical Committee 3: Fire safety of steel structures. (1983). *European recommendations for the fire safety of steel structures*. Amsterdam, the Netherlands: Elsevier.

19. Kamikawa, N., Sato, K., Miyamoto, G., Muruyama, M., Sekido, N., Tsuzaki, K., and Furuhashi, T. (2015). Stress-strain behaviour of ferrite and bainite with nano-precipitation in low carbon steels. *Acta Materialia*, 83, 383–396.
20. Liu, Q., Huang, X., Lloyd, D.J., and Hansen, N. (2002). Microstructure and strength of commercial purity aluminium (AA 1200) cold rolled to large strains. *Acta Materialia*, 50, 3789–3802.
21. Sha, W. and Kelly, F.S. (2004). Atom probe field ion microscopy study of commercial and experimental structural steels with fire resistant microstructures. *Materials Science and Technology*, 20(4), 449–457.
22. Dere, E.G., Sharma, H., Petrov, R.H., Sietsma J., and Offerman, S.E. (2013). Effect of Niobium and grain boundary density on fire-resistance of Fe-C-Mn steel. *Scripta Materialia*, 68(8), 651–654.
23. Sha, W., Kelly, F.S., and Guo, Z.X. (1999). Microstructure and properties of Nippon fire-resistant steels. *Journal of Materials Engineering and Performance*, 8(5), 606–612.
24. Lacroix, G., Pardoën, T., and Jacques, P.J. (2008). The fracture toughness of TRIP-assisted multiphase steels. *Acta Materialia*, 56, 3900–3913.
25. Morhbacher, H. (2013). Reverse metallurgical engineering towards sustainable manufacturing of vehicles using Nb and Mo alloyed high performance steels. *Advances in manufacturing*, 1(1), 28–41.
26. Seto, K. and Matsuda, H. (2013). Application of nanoengineering to research and development and production of high strength steel sheets. *Materials Science and Technology*, 29(10), 1158–1165.
27. Jang, J.H., Heo, Y.U., Lee, C.H., Bhadeshia, H.K.D.H., and Suh, D.W. (2013). Interphase precipitation in Ti-Nb and Ti-Nb-Mo bearing steel. *Materials Science and Technology*, 29(3), 309–313.
28. Jang, J.H., Lee, C.H., Heo, Y.U., and Suh, D.W. (2012). Stability of (Ti,M)C (M=Nb, V, Mo and W) carbide in steels using first-principles calculations. *Acta Materialia*, 60, 208–217.
29. Chen, C.Y., Chen, C.C., and Yang, J.R. (2014). Microstructure characterization of nanometer carbides heterogeneous precipitation in Ti-Nb and Ti-Nb-Mo steel. *Materials Characterisation*, 88, 69–79.
30. Gladman, T. (1999). Precipitation hardening in metals. *Materials Science and Technology*, 15(1), 30–36.
31. Martin J.W. (1998). *Precipitation hardening* (2nd ed.). Oxford, UK: Butterworth-Heinemann.
32. Martin J.W. (1998). *Precipitation hardening* (2nd ed.). Oxford, UK: Butterworth-Heinemann.
33. Gladman, T. (2002). *The physical metallurgy of microalloyed steels*. London, UK: Maney Publishing.
34. Kamikawa, N., Abe, Y., Miyamoto, G., Funakawa, Y., and Furuhashi, T. (2014). Tensile behaviour of Ti,Mo-added low carbon steels with interphase precipitation. *ISIJ International*, 54(1), 212–221.
35. Chen, M.Y., Gouné, M., Verdier, M., Bréchet, Y., and Yang, J.R. (2014). Interphase precipitation in vanadium-alloyed steels: strengthening

- contribution and morphological variability with austenite to ferrite phase transformation. *Acta Materialia*, 64, 78–92.
36. Baker, T.N. (2009). Processes, microstructure and properties of vanadium microalloyed steels. *Materials Science and Technology*, 25(9), 1083–1107.
 37. Medina, S.F., Quispe, A., and Gómez M. (2003). Strain induced precipitation effect on austenite static recrystallisation in microalloyed steels. *Materials Science and Technology*, 19(1), 99–108.
 38. Ishikawa F., Takahashi, T., and Ochi, T. (1994). Intragranular ferrite nucleation in medium-carbon vanadium steels. *Metallurgical and Materials Transactions A*, 25(5), 929–936.
 39. Medina, S.F., Gómez, M., and Rancel L. (2008). Grain refinement by intragranular nucleation of ferrite in a high nitrogen content vanadium microalloyed steel. *Scripta Materialia*, 58(12), 1110–1113.
 40. Furuhashi, T., Yamaguchi, J., Sugita, N., Miyamoto, G., and Maki, T. (2003). Nucleation of proeutectoid ferrite on complex precipitates in austenite. *ISIJ International*, 43(10), 1630–1639.
 41. Glodowski, R.J. (2002). *Experience in producing vanadium-microalloyed steels*. Paper presented at the International Symposium on Thin-Slab Casting and Rolling, Guangzhou, China.
 42. Karmakar, A., Mandal A., Mukherjee, S., Kundu, S., Srivastava, D., Mitra, R., and Chakrabarti, D. (2016). Effect of isothermal holding temperature on the precipitation hardening in vanadium-microalloyed steels with varying carbon and nitrogen levels. ArXiv:1607.02721.
 43. Korchynsky M. and Stuart H. (1970) The role of strong carbide and sulfide forming elements in the manufacture of formable high strength low alloy steels. *Proceedings of the Symposium on low alloy high strength steels*. 17–27. Nuremberg, Germany: Metallurgical Companies.
 44. Zhang, Y.J., Miyamoto, G., Shinbo, K., and Furuhashi, T. (2013). Effects of α/γ orientation relationship on VC interphase precipitation in low-carbon steels. *Scripta Materialia*, 69(1), 17–20.
 45. Morales E.V., Gallego J., and Kestenbach H.J. (2003). On coherent carbonitride precipitation in commercial microalloyed steels. *Philosophical Magazine Letters*, 83(2), 79–87.
 46. Nöhler, M., Zamberger, S., Primiga, S., and Leitner H. (2013). Atom probe study of vanadium interphase precipitates and randomly distributed precipitates in ferrite. *Micron*, 54–55, 57–64.
 47. Zhang, Y.J., Miyamoto, G., Shinbo, K., and Furuhashi, T. (2017). Quantitative measurements of phase equilibria at migrating α/γ interface and dispersion of VC interphase precipitates: Evaluation of driving force for interphase precipitation. *Acta Materialia*, 128, 166–175.
 48. Baker, T.N. (2016). Microalloyed steels. *Ironmaking and steelmaking*, 43(4), 264–307.
 49. Chen, J., Lu, M., Tang, S., Liu, Z., and Wang, G. (2014). Influence of cooling paths on microstructural characteristics and precipitation behaviours in a low carbon V-Ti microalloyed steel. *Materials Science and Engineering A*, 594, 389–393.

50. Kamikawa, N., Hirohashi, M., Sato, Y., Chandiran, E., Miyamoto, G., and Furuhashi, T. (2015). Tensile behaviour of ferrite-martensite dual phase steels with nano-precipitation of vanadium carbides. *ISIJ International*, 55(8), 17811–1790.
51. Zajac, S., Siwecki, T., Hutchinson, B., and Atlegård, M. (1991). Recrystallisation controlled rolling and accelerated cooling for high strength and toughness in V-Ti-N steels. *Metallurgical and Material Transactions A*, 22(11), 2681–2694.
52. Zhang, J., Wang, F.M., Yang, Z.B., and Li, C.R. (2016). Microstructure, precipitation and mechanical properties of V-N-alloyed steel after different cooling processes. *Metallurgical and Materials Transactions A*, 47(12), 6621–6631.
53. Li, Y. and Milbourn, D. (2015). The influence of vanadium microalloying on the production of thin slab casting and direct rolled steel strip. *HSLA Steels 2015, Microalloying 2015 and Offshore Engineering Steels 2015*. Hangzhou, Zhejiang Province, China: The Chinese Society for Metals and Chinese Academy of Engineering.
54. Staško, R., Adrian, H., and Adrian, A. (2006). Effect of nitrogen and vanadium on austenite gain growth kinetics of a low alloy steel. *Materials Characterisation*, 56(4–5), 340–347.
55. White, M.J. and Owen, W.S. (1980). Effects of vanadium and nitrogen on recovery and recrystallisation during and after hot-working some HSLA steels. *Metallurgical and Material Transactions A*, 11(4), 597–604.
56. Andrade, H.L., Akben, M.G., and Jonas, J. J. (1983). Effect of Molybdenum, Niobium and Vanadium on static recovery and recrystallisation and on solute strengthening in microalloyed steels. *Metallurgical and Material Transactions A*, 14(10), 1967–1977.
57. Jonas, J.J. (1984). Mechanical testing for the study of austenite recrystallization and carbonitride precipitation. In D.P. Dunne and T. Chandra (Eds.), *Conference on High Strength Low Alloy Steels*. Wollongong, Australia: University of Wollongong.
58. García-Mateo, C., López, B., and Rodríguez-Ibabe, J.M. (2001). Static recrystallisation kinetics in warm worked vanadium microalloyed steels. *Materials Science and Engineering A*, 303(1–2), 216–225.